Commun. Comput. Phys.
doi: 10.4208/cicp.060313.300514a

Vol. **16**, No. 4, pp. 1116-1134
October 2014

A Multi-Domain Hybrid DG and WENO Method for Hyperbolic Conservation Laws on Hybrid Meshes

Jian Cheng[1] and Tiegang Liu[1,*]

[1] *LMIB, School of Mathematics and Systems Science, Beihang University, Beijing 100191, P.R. China.*

Received 6 March 2013; Accepted (in revised version) 30 May 2014

Available online 21 August 2014

Abstract. In [SIAM J. Sci. Comput., 35(2)(2013), A1049–A1072], a class of multi-domain hybrid DG and WENO methods for conservation laws was introduced. Recent applications of this method showed that numerical instability may encounter if the DG flux with Lagrangian interpolation is applied as the interface flux during the moment of conservative coupling. In this continuation paper, we present a more robust approach in the construction of DG flux at the coupling interface by using WENO procedures of reconstruction. Based on this approach, such numerical instability is overcome very well. In addition, the procedure of coupling a DG method with a WENO-FD scheme on hybrid meshes is disclosed in detail. Typical testing cases are employed to demonstrate the accuracy of this approach and the stability under the flexibility of using either WENO-FD flux or DG flux at the moment of requiring conservative coupling.

AMS subject classifications: 65M60, 65M99, 35L65

Key words: Discontinuous Galerkin method, weighted essentially nonoscillatory scheme, hybrid method, conservation laws.

1 Introduction

To maintain reliability of solution, high order methods with low diffusion and low dissipation have become necessary when the structure of solution is complex and the resolution of traditional second order methods is not satisfactory. With this regard, high order methods have been widely developed in solving nonlinear hyperbolic conservation laws in recent years.

The first type is the high order finite difference (FD) schemes, for instance, the weighted essentially non-oscillatory finite difference (WENO-FD) schemes [7, 8]. The

*Corresponding author. *Email addresses:* chengjian@smss.buaa.edu.cn (J. Cheng), liutg@buaa.edu.cn (T. G. Liu)

 ©2014 Global-Science Press

obvious advantages of a WENO-FD schemes are highly efficient and easy to achieve high order accuracy in structure meshes. It has usually been used in the direct numerical simulation (DNS) of turbulence or in the area of computational aeroacoustics (CAA) where high order accuracy plays a significant role. Nevertheless, the difficulty in handling complex geometries for this type of schemes limits their practical application. The second type of high order methods belongs to high order finite volume (FV) schemes, such as the weighted essentially non-oscillatory finite volume (WENO-FV) schemes [9] and high order k-exact finite volume methods [10]. This type of methods has flexibility in handling almost arbitrary mesh and geometry which makes them dominant in the CFD community. However, when it extends to high order accuracy, the implementation of a FV type schemes usually becomes much involved since the number of cells used for reconstruction increases tremendously when the accuracy order goes higher. The last type is the high order discontinuous Galerkin (DG) type methods, which include the traditional Runge-Kutta discontinuous Galerkin (RKDG) methods developed by Cockburn and Shu [1–3], the Spectral volume/difference (SV/SD) methods introduced by Wang et al. [19–21] and the correction procedure via reconstruction (CPR) schemes recently introduced by Huynh [22]. The DG type methods can fit for complex geometries in a more flexible way and are compact as each element only communicates with its immediate face-neighbors through approximate Riemann solvers. In DG type methods, one important component is the construction of nonlinear limiters, see related work [4–6] for reference. Unfortunately, this type of methods also suffers some not well solved issues and weaknesses, such as high computational cost and difficulties in developing more reliable nonlinear limiters. These become major bottlenecks for DG methods in practical applications.

All of those high order methods mentioned above have their advantages and disadvantages. In order to overcome the disadvantages of a specific type of methods, hybrid methods which combine the advantages of two different kinds of high order methods have been proposed. There are mainly two kinds of hybrid approaches presented in literatures for solving Euler equations, one is based on local polynomial reconstruction, the other is based on computational domain decomposition.

Balsara et al. [11] adopted the first approach and presented a novel class of hybrid RKDG and Hermite WENO schemes on structured grids. Their hybrid algorithm stores cell averages as well as slopes for each cell of the RKDG methods and reconstructs high order degrees of freedom through Hermite reconstruction. Luo et al. [12, 13] introduced a reconstructed DG method (RDG) for Euler equations on arbitrary grids. In contrast to the traditional RKDG methods, RDG reconstructs high order degrees of freedom using a least-squares technique. The idea behind this hybrid approach is to combine the efficiency of the reconstruction methods widely used in FV methods and the accuracy and robustness of DG methods. Dumbser et al. [14] presented a unified framework for constructing one step finite volume and discontinuous Galerkin schemes on unstructured meshes, resulting in a class of $P_N P_M$ schemes. This approach yields two special cases: classical high order finite volume methods ($N = 0$) and DG methods ($N = M$). Very

recently, Zhang et al. [15–17] introduced a hybrid DG/FV method based on hybrid reconstruction approaches which were named 'dynamic reconstruction' and 'static reconstruction'. In their hybrid DG/FV method, a DG method based on Taylor basis functions was adopted to compute the low order degrees of freedom. A high order finite volume method is then used to reconstruct high order derivatives with the known low order derivatives.

Based on the approach of computational domain decomposition, a multi-domain hybrid spectral-WENO method was introduced by Costa et al. [23] for hyperbolic conservation laws. The hybrid spectral-WENO method conjugates the non-oscillatory properties of the high order WENO schemes and the high efficiency and accuracy of spectral methods in a multi-domain approach. Recently, Shahbazi et al. [24] introduced a multi-domain Fourier-continuation/WENO hybrid solver for conservation laws. He et al. [18] developed a hybrid FE/FV scheme which adopts a DG method near solid wall and a traditional second order finite volume method elsewhere. In the area of CAA, Utzmann et al. [26,27] and Léger et al. [28] developed a coupled DG/FD solver for linearized Euler equations. The coupled DG/FD solver can approximate the solution in the close neighborhood of complex obstacles on an unstructured DG mesh and compute the rest of the field on a Cartesian FD grid in order to alleviate computational time and resources.

In our previous work [25], a class of multi-domain hybrid DG and WENO methods for conservation laws was introduced. Two versions of the multi-domain hybrid DG and WENO methods were developed: one version is the hybrid DG/WENO-FV method, the other is the hybrid DG/WENO-FD method. It seems unusual to combine an averaged-value based DG method with a point-value based WENO-FD scheme in a domain decomposition approach. Theoretical analysis had shown that the conservative coupling approach deteriorates the accuracy seriously and only the non-conservative coupling approach can preserve high order accuracy at the coupling interface. Thus, a special treatment was developed in the previous work: the non-conservative coupling approach is employed when the solution is smooth enough and it is replaced by the conservative coupling approach when there are possible discontinuities passing through the interface. In our previous work, we recommended WENO-FD flux as the sole interface flux during the moment of conservative coupling. Recent applications showed that numerical instability can occur if the DG flux presented in [25] is applied at the interface during the moment of conservative coupling. The cause of this instability lies in the reconstruction procedure based on a direct Lagrangian interpolation as proposed in our previous work. The direct Lagrangian interpolation approach was found unable to provide reliable values in recovering the degrees of freedom for a DG solution in target cells if there is a strong discontinuity in the interpolation stencil.

In this paper, we introduce a more reliable approach of reconstructing DG flux based on WENO interpolation. Compared to the previous Lagrangian interpolation, the new approach is more robust and stable. This also provides us a flexible choice of using either WENO-FD flux or DG flux during the moment of conservative coupling. Numerical results to be given later show there are indeed no much difference using either DG flux

or WENO-FD flux with the new approach. In addition, we present in detail the concrete implementation of the hybrid DG/WENO-FD method for hyperbolic conservation laws on hybrid meshes for the convenience of potential users in this work.

The rest of this paper is arranged as follows. In Section 2, we give a brief introduction of the traditional DG method and the WENO-FD scheme. In Section 3, we present the multi-domain hybrid DG/WENO-FD method for two dimensional conservation laws on hybrid meshes. To verify the performance of the multi-domain hybrid method, various numerical tests are presented in Section 4. Finally, concluding remarks and suggestions for future work are given in Section 5.

2 Brief review of DG method and WENO-FD scheme

In this section, we use the following two dimensional scalar hyperbolic conservation law to give a brief review of the DG method and the WENO-FD scheme:

$$\begin{cases} u_t+f(u)_x+g(u)_y=0, \\ u(x,y,0)=u_0(x,y), \qquad (x,y)\in\Omega\times(0,T). \end{cases} \tag{2.1}$$

2.1 Review of DG method

Define a given domain Ω which is divided into a collection of non-overlapping cells Ω_e. For the traditional DG method, the space of solution as well as the test function is given by $V_h^k=\{v(x,y):v(x,y)|_{\Omega_e}\in P^k(\Omega_e)\}$, $P^k(\Omega_e)$ denotes a set of polynomials of degree equal or less than k. In each cell Ω_e, the numerical solution can be expressed as a piecewise polynomial consists of several specific basis functions:

$$u^h(x,y,t)=\sum_{l=0}^{k}u^{(l)}(t)v_{(l)}(x,y), \qquad (x,y)\in\Omega_e, \tag{2.2}$$

where $\{v_{(l)}(x,y),l=0,\cdots,k\}$ are local basis functions in Ω_e. A set of local orthogonal basis [4] is adopted in this paper. With the orthogonality property of the basis, the degrees of freedom $u^{(l)}$ in Ω_e can be written as:

$$u^{(l)}(t)=\frac{1}{w_l}\int_{\Omega_e}u^h(x,y,t)v_{(l)}(x,y)dxdy, \qquad l=0,\cdots,k, \tag{2.3}$$

where $w_l=\int_{\Omega_e}(v_{(l)}(x,y))^2dxdy$.

In order to determine the approximate solution, the DG method evolves the degrees of freedom $u^{(l)}(t)$ with following differential equation which is obtained by multiplying

the origin equation (2.1) with $v_{(l)} \in V_h^k$ and integrating by parts:

$$\frac{d}{dt}u^{(l)}(t) = \frac{1}{w_l}\left(\int_{\Omega_e}\left(f(u^h(x,y,t))\frac{\partial}{\partial x}v_{(l)}(x,y) + g(u^h(x,y,t))\frac{\partial}{\partial y}v_{(l)}(x,y)\right)dxdy \right.$$
$$\left. - \int_{\partial\Omega_e}(f(u^h(x,y,t)),g(u^h(x,y,t)))^T \cdot \mathbf{n}_{\partial\Omega_e} \cdot v_{(l)}(x,y)ds\right), \quad l=0,\cdots,k, \quad (2.4)$$

where $\mathbf{n}_{\partial\Omega_e}$ is the outward unit normal of edge $\partial\Omega_e$.

In (2.4), the integral terms can be computed by suitable numerical quadratures up to $2k$ for the element volume integral and up to $2k+1$ for the edge integral. As $u^h(x,y,t)$ is discontinuous at cell interfaces of Ω_e, the flux $(f(u^h(x,y,t)),g(u^h(x,y,t)))^T \cdot \mathbf{n}_{\partial\Omega_e}$ is replaced by a monotone numerical flux $h_{\partial\Omega_e}(u^-,u^+)$. In this paper, we simply use the following Lax-Friedrichs flux as follow:

$$h_{\partial\Omega_e}(u^-,u^+) = \frac{1}{2}\left(\mathbf{f}(u^-)\cdot\mathbf{n}_{\partial\Omega_e} + \mathbf{f}(u^+)\cdot\mathbf{n}_{\partial\Omega_e} - \alpha_{\partial\Omega_e}(u^+-u^-)\right), \quad (2.5)$$

where $\mathbf{f}(u) = (f(u),g(u))^T$ and $\alpha_{\partial\Omega_e,n} = |\partial\mathbf{f}(u)/\partial u \cdot \mathbf{n}_{\partial\Omega_e}|$.

If there are strong discontinuities in solutions, the method above generates significant oscillation and even becomes nonlinearly unstable. To avoid such difficulties, a nonlinear TVD(TVB) [3] or WENO type limiter [4–6] must be employed to suppress numerical oscillation.

2.2 Review of WENO-FD scheme

The WENO-FD scheme for two dimensional conservation laws is based on conservative approximation to derivatives from point values. Uniform grid is generally required and spatial derivatives of (2.1) are approximated as follow:

$$\frac{du_{i,j}(t)}{dt} = -\frac{1}{\Delta x}(\hat{f}_{i+\frac{1}{2},j} - \hat{f}_{i-\frac{1}{2},j}) - \frac{1}{\Delta y}(\hat{g}_{i,j+\frac{1}{2}} - \hat{g}_{i,j-\frac{1}{2}}). \quad (2.6)$$

The numerical fluxes $\hat{f}_{i+1/2,j}$ and $\hat{g}_{i,j+1/2}$ are obtained by the one dimensional WENO-FD reconstruction procedure. Next, we fix $y=y_j$ and give a review of the reconstruction procedure for $\hat{f}_{i+1/2,j}$ in the x-axis direction. For convenience, subscript 'j' is omitted in the following description. It should be noted that the reconstruction in the y-axis direction is similar.

The spatial derivative in the x-axis direction of Eq. (2.1) can be replaced by the following divided difference exactly

$$\frac{\partial f(u)}{\partial x}|_{x=x_i} = \frac{1}{\Delta x}\left(h(x_{i+\frac{1}{2}}) - h(x_{i-\frac{1}{2}})\right), \quad (2.7)$$

where the definition of $h(x)$ is:

$$f(x)=\frac{1}{\Delta x}\int_{x-\Delta x/2}^{x+\Delta x/2}h(\xi)d\xi. \tag{2.8}$$

The WENO-FD scheme approximates $h(x)$ which is denoted by $\widehat{f}(x)$ through reconstructing an interpolation polynomial with known point values of $f(u)$. We use a fifth-order WENO-FD scheme as an example to illustrate the procedure. In a fifth-order WENO-FD scheme, the numerical flux $\widehat{f}_{i+1/2}$ is built through a convex combination of three quadratic interpolation polynomials $q^k(x)$,$k=0,1,2$ in three stencils S^0,S^1,S^2, where $S^0=\{f_{i-2},f_{i-1},f_i\}$, $S^1=\{f_{i-1},f_i,f_{i+1}\}$ and $S^2=\{f_i,f_{i+1},f_{i+2}\}$. The numerical flux is evaluated with

$$\widehat{f}_{i+\frac{1}{2}}=\sum_{k=0}^{2}w_kq^k(x_{i+\frac{1}{2}}), \tag{2.9}$$

where w_k is the nonlinear weight of stencil k which satisfies

$$\sum_{k=0}^{2}w_k=1,\qquad w_k\geq 0,\qquad k=0,1,2. \tag{2.10}$$

The fifth-order WENO-FD scheme uses the following form of nonlinear weights

$$w_k=\frac{\alpha_k}{\sum_{s=0}^{2}\alpha_s},\qquad \alpha_k=\frac{d_k}{(\varepsilon+\beta_k)^2},\qquad k=0,1,2, \tag{2.11}$$

where d_k is the linear weight of stencil k and β_k is the smoothness indicator [7]

$$\beta_k=\sum_{l=1}^{2}\int_{x_{i-\frac{1}{2}}}^{x_{i+\frac{1}{2}}}\Delta x^{2l-1}\left(\frac{\partial^l q^k(x)}{\partial^l x}\right)^2dx,\qquad k=0,1,2. \tag{2.12}$$

In regions of smooth solution, the interpolation polynomial at the cell interface $x_{i+1/2}$ follows

$$\begin{aligned}\widehat{f}_{i+\frac{1}{2}}&=\frac{1}{60}(2f_{i-2}-13f_{i-1}+47f_i+27f_{i+1}-3f_{i+2})\\&=h_{i+\frac{1}{2}}+\mathcal{O}(\Delta x^5),\end{aligned} \tag{2.13}$$

in the stencil $S=\{f_{i-2},f_{i-1},f_i,f_{i+1},f_{i+2}\}$ to achieve fifth order of accuracy. In regions which contain discontinuities, the nonlinear weights are assigned to preserve that the solution is essentially non-oscillatory. The numerical flux $\hat{g}_{i,j+1/2}$ in the y-axis direction can be achieved in a similar approach.

3 Multi-domain hybrid DG and WENO-FD method on hybrid meshes

From now on, we start to introduce our multi-domain hybrid DG and WENO-FD (DG/WENO-FD) method. In this section, we will focus on its implementation for the two dimensional scalar conservation law:

$$\begin{cases} u_t + f(u)_x + g(u)_y = 0, \\ u(x,y,0) = u_0(x,y), \qquad (x,y) \in \Omega \times (0,T). \end{cases} \tag{3.1}$$

For the domain decomposition, we give an example in Fig. 1(a). As in Fig. 1(a), the computational domain is divided into two subdomains which the left subdomain is handled by the unstructured DG method and the right is applied by the WENO-FD scheme. At the coupling interface denoted by $x = x_{I+1/2,J}$, we assume the boundary size of a triangle element of the unstructured mesh is equal to the size of a rectangle element in the structured mesh, as shown in Fig. 1(b).

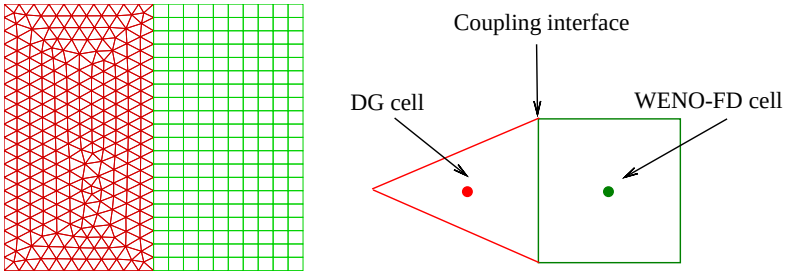

(a) Sample hybrid mesh (b) Zoom in hybrid interface

Figure 1: Multi-domain hybrid DG/WENO-FD method on hybrid meshes.

The key issue of the multi-domain hybrid DG/WENO-FD method is the treatment of numerical fluxes at the coupling interface in order to preserve high order accurate for smooth solutions as well as keep robustness in handling discontinuities, such as shock waves. From our experience of previous work in one dimensional hybrid methods, we found that conservative coupling between an averaged-value based DG method and a point-value based WENO-FD scheme deteriorates the order of accuracy seriously. Here, the conservative coupling means that at the coupling interface there is an unique numerical flux defined. Furthermore, we have shown that a conservative hybrid DG and WENO-FD scheme is of first order accuracy for smooth solutions. Thus, non-conservative hybrid approach has to be adopted in order to maintain high order accuracy, we need to construct numerical fluxes for the DG method and the WENO-FD scheme at the coupling interfaces, respectively. Next, we will use the multi-domain coupling of a third-order DG method with a fifth-order WENO-FD scheme as an example to illustrate the procedure.

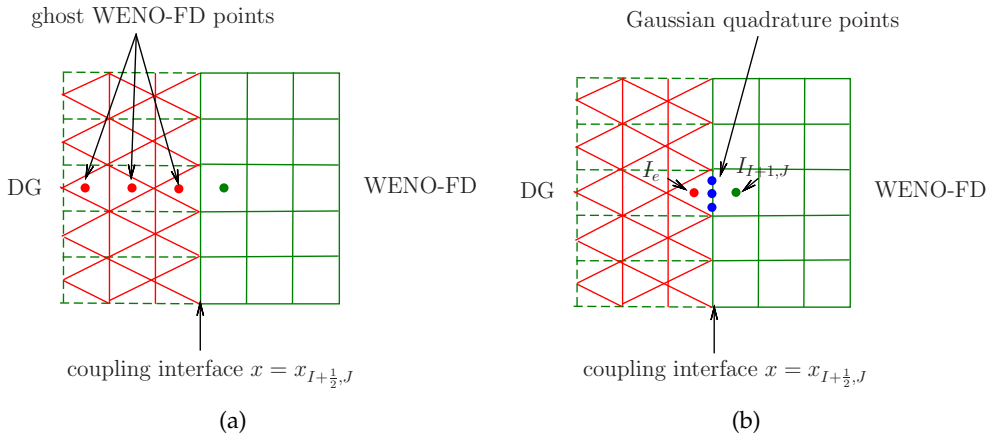

Figure 2: Flux construction of hybrid DG/WENO-FD method on hybrid meshes.

First, we focus on the construction of a WENO-FD flux at the coupling interface in the x-axis direction. To construct the numerical flux at the interface $x=x_{I+1/2,J}$, the DG subdomain can provide the appropriate point values for the WENO-FD scheme. More specifically, for the construction of $\tilde{f}^{(weno)}_{I+1/2,J}$, we need point values $u^{(weno)}_{I-2,J}$, $u^{(weno)}_{I-1,J}$, $u^{(weno)}_{I,J}$ at ghost points $x_{I-2,J}$, $x_{I-1,J}$, $x_{I,J}$ inside the DG subdomain. In this work, $u^{(weno)}_{I-2,J}$, $u^{(weno)}_{I-1,J}$, $u^{(weno)}_{I,J}$ are simply calculated from the approximate polynomials provided from the DG method at those cells as shown in Fig. 2(a).

Next, we present the procedure of constructing a DG flux at the coupling interface $x=x_{I+1/2,J}$. In the construction of a DG flux, we need to get the values of three Gaussian quadrature points at the edge of coupling interface in Fig. 2(b). At each Gaussian quadrature point, we need $u^{\pm}$, the u^{-} can be calculated from the DG solutions.

The u^{+} was obtained via direct Lagrangian interpolation in our previous work [25]. Recently we found that such approach may generate numerical instability in some situation. In this work, we give a more robust and stable approach to obtain these Gaussian quadrature point values through the idea of WENO interpolation. Below is the detailed steps of obtaining u^{+} at these Gaussian quadrature points of the coupling interfaces:

Step 1: Choose a stencil $S=\{u_{i,j}: i=I-1,I,\cdots,I+3; j=J-2,J-1,\cdots,J+2\}$.

Step 2: Perform two dimensional WENO interpolation in the stencil S through a dimension by dimension approach and get the three Gaussian quadrature point values respectively, at $x_G=x_{I+\frac{1}{2},J-\frac{1}{2}\sqrt{\frac{3}{5}}}$, $x_G=x_{I+\frac{1}{2},J}$ and $x_G=x_{I+\frac{1}{2},J+\frac{1}{2}\sqrt{\frac{3}{5}}}$ of the coupling interface $x=x_{I+1/2,J}$.

Here, we use an example to explain the two dimensional WENO interpolation in detail. In order to get the point value at $x_G=x_{I+\frac{1}{2},J-\frac{1}{2}\sqrt{\frac{3}{5}}}$ through dimension by dimension implementation, we need to obtain the point values at $x_G=x_{i,J-\frac{1}{2}\sqrt{\frac{3}{5}}}$, $i=I-1,I,\cdots,I+3$ in

the x-axis direction, respectively. They are obtained by WENO interpolation along the y-axis direction. Below is the detailed procedures of calculating each Gaussian quadrature point value at $x_G = x_{i,J-\frac{1}{2}\sqrt{\frac{3}{5}}}$, $i = I-1, I, \cdots, I+3$ through the WENO interpolation in the y-axis direction.

Step (2.1): Identify the stencil $S_i = \{u_{i,j} : j = J-2, J-1, \cdots, J+2\}$ and divide it into three small stencil $S_i^{(0)} = \{u_{i,j} : j = J-2, J-1, J\}$, $S_i^{(1)} = \{u_{i,j} : j = J-1, J, J+1\}$ and $S_i^{(2)} = \{u_{i,j} : j = J, J+1, J+2\}$.

Step (2.2): Construct interpolation polynomial $p^{(r)}(x)$ in each stencil $S_i^{(r)}$, $r = 0,1,2$ which satisfies $p^{(r)}(x_{i,j}) = u_{i,j}$, for x_G we have

$$p^{(0)}(x_G) = \frac{43-6\sqrt{15}}{40} u_{i,J} - \frac{6-8\sqrt{15}}{40} u_{i,J-1} + \frac{3-2\sqrt{15}}{40} u_{i,J-2}, \tag{3.2a}$$

$$p^{(1)}(x_G) = \frac{3-2\sqrt{15}}{40} u_{i,J+1} + \frac{34}{40} u_{i,J} + \frac{43+6\sqrt{15}}{40} u_{i,J-1}, \tag{3.2b}$$

$$p^{(2)}(x_G) = \frac{3+2\sqrt{15}}{40} u_{i,J+2} - \frac{6+4\sqrt{15}}{40} u_{i,J+1} + \frac{43+6\sqrt{15}}{40} u_{i,J}. \tag{3.2c}$$

Step (2.3): Calculate the linear weights λ_r, smoothness indicator β_r and nonlinear weights w_r for each stencil $S_i^{(r)}$ $r = 0,1,2$ by following the procedures described in Section 2.2, here for the Gaussian quadrature point x_G, we have the linear weights

$$\lambda_0 = -\frac{17(3+4\sqrt{15})}{240(3-2\sqrt{15})}, \qquad \lambda_1 = 1.0 - \lambda_0 - \lambda_2, \qquad \lambda_2 = \frac{17(-3+4\sqrt{15})}{240(3+2\sqrt{15})}. \tag{3.3}$$

Step (2.4): Get the WENO interpolation value at the target Gaussian quadrature point where

$$u_G^+ \approx \sum_{r=0}^{3} w_r p^{(r)}(x_G). \tag{3.4}$$

Step 3: Obtain the DG flux $\widehat{f}^{(dg)}_{I+1/2,J}$ using the formula Eq. (2.5).

Compared with the procedures based on the direct Lagrangian interpolation in our previous work, this new approach based on WENO interpolation can provide the approximated Gaussian quadrature point values with essentially non-oscillatory property. Thus, it is more robust and enhances the stability of the conservative coupling approach when DG flux is adopted at the coupling interface. As a result, the DG flux $\widehat{f}^{(dg)}_{I+1/2,J}$ becomes a new possible choice for the conservative coupling at the coupling interface. It should be noted that although the description of above procedures is based on two dimensional scalar equation, we can extend the above procedures of WENO interpolation to two dimensional Euler equations easily through a component-wise approach or a characteristic-wise approach.

There are two numerical fluxes: $\tilde{f}^{(weno)}_{I+1/2,J}$ and $\widehat{f}^{(dg)}_{I+1/2,J}$ at the coupling interface. In general, $\tilde{f}^{(weno)}_{I+1/2,J}$ is not equal to $\widehat{f}^{(dg)}_{I+1/2,J}$, thus the scheme is non-conservative. Numerical results show that the non-conservative hybrid DG/WENO-FD method above can preserve third order accuracy for smooth solutions.

The non-conservative hybrid DG/WENO-FD method can handle smooth solutions well, however, when a discontinuity passes through the coupling interface, the non-conservative approach suffers a serious loss in conservation and leads to inaccurate results. Conservation must be preserved at this time in order to avoid such numerical inaccuracy. In order to detect a possible discontinuity approaching the coupling interface, a natural way is to use a so-called 'trouble cell indicators' in the interpolation stencil S. Trouble cell is the cell which discontinuities may appear and limiting procedure is needed. If the interpolation stencil contains a trouble cell, it is wise to use conservative coupling approach instead of non-conservative one at the coupling interface. That means the non-conservative hybrid method comes back to be conservative when discontinuities are approaching the coupling interface. Here, we use a TVD(TVB) trouble cell indicator to detect possible discontinuities and the details are as follow:

We denote $\bar{u}_e,\bar{u}_{I+1,J},\bar{u}_{I+2,J}$ as volume averaged values of the cells $I_e,I_{I+1,J},I_{I+2,J}$ as shown in Fig. 2(b). Here, $\bar{u}_{I+1,J},\bar{u}_{I+2,J}$ are got through the integration of $p(x,y)$ and $\bar{u}_e$ is the zero degree of freedom of DG solution at I_e. Define $u^G_{I+1/2,J}$, $G=0,1,2$ are the Gaussian quadrature point values reconstructed using WENO-FD point values at the coupling interface,

$$\tilde{u}^G_{I+\frac{1}{2},J}=\bar{u}_{I+1,J}-u^G_{I+1/2,J},\quad \Delta u^+_{I+\frac{1}{2},J}=\bar{u}_{I+2,J}-\bar{u}_{I+1,J},\quad \Delta u^-_{I+\frac{1}{2},J}=\bar{u}_{I+1,J}-\bar{u}_e. \tag{3.5}$$

By applying a TVD(TVB) minmod function at the coupling interface

$$m(a_1,a_2,a_3)=\begin{cases} s\cdot\min\{|a_1|,|a_2|,|a_3|\}, & \text{if } sign(a_1)=sign(a_2)=sign(a_3)=s,\\ 0, & \text{otherwise,}\end{cases} \tag{3.6}$$

we can get the modified $\tilde{u}^{G(mod)}_{I+\frac{1}{2},J}$ as

$$\tilde{u}^{G(mod)}_{I+\frac{1}{2},J}=m(\tilde{u}^G_{I+\frac{1}{2},J},\Delta u^+_{I+\frac{1}{2},J},\Delta u^-_{I+\frac{1}{2},J}). \tag{3.7}$$

If $\tilde{u}^{G(mod)}_{I+1/2,J}\neq\tilde{u}^G_{I+1/2,J}$ for any Gaussian quadrature point, then there is a possible discontinuity approaching the coupling interface and the conservative coupling approach is applied at this time.

Finally, we summary the procedure of the multi-domain hybrid DG/WENO-FD method in following steps:

Step 1: Initialize degrees of freedom for the DG subdomain and point values for the WENO-FD subdomain;

Step 2: Construct numerical fluxes $\tilde{f}^{(weno)}_{I+1/2,J}$ and $\widehat{f}^{(dg)}_{I+1/2,J}$ at the coupling interface for the DG and the WENO-FD subdomain, respectively;

Step 3: Use discontinuity indicator to identify possible discontinuities at the coupling interface: if $\tilde{u}^{G(mod)}_{I+1/2,J}=\tilde{u}^G_{I+1/2,J}$, $G=0,1,2$, the non-conservative coupling approach is adopted at the coupling

interface; otherwise, the conservative coupling method is applied and an unique numerical flux $\tilde{f}^{(weno)}_{I+1/2,J}$ or $\widehat{f}^{(dg)}_{I+1/2,J}$ is used at the coupling interface;

Step 4: Form the space discretization for the DG and the WENO-FD subdomain.

As for time discretization, an explicit third-order TVD Runge-Kutta method is used:

$$u^{(1)} = u^n + \Delta t L(u^n), \tag{3.8a}$$

$$u^{(2)} = \frac{3}{4}u^n + \frac{1}{4}u^{(1)} + \frac{1}{4}\Delta t L(u^{(1)}), \tag{3.8b}$$

$$u^{n+1} = \frac{1}{3}u^n + \frac{2}{3}u^{(2)} + \frac{2}{3}\Delta t L(u^{(2)}). \tag{3.8c}$$

As the CFL number of a third-order RKDG method and a fifth-order WENO-FD schemes is required to be 0.18 and 0.6, respectively. Thus, we take the CFL number equal to 0.18 for our hybrid DG/WENO-FD method for the purpose of stability. In the next section, we will demonstrate the performance of the hybrid DG/WENO-FD method for two dimensional conservation laws.

4 Numerical results

4.1 Two dimensional scalar cases

Example 4.1. We test the accuracy of the hybrid DG/WENO-FD method to solve a two dimensional linear advection equation with the following initial and periodic boundary conditions. The subdomain interface is set at $x=0.5, 0.0<y<1.0$ where the unstructured DG method is applied in $[0.0,0.5]\times[0.0,1.0]$ and the structured WENO-FD scheme is employed in $[0.5,1.0]\times[0.0,1.0]$. The computing time is till 1.0. We display the L_∞ and L_1 errors of DG and WENO-FD subdomains, respectively. The computing result is shown in Table 1 with excepted accuracy.

$$\begin{cases} u_t + u_x + u_y = 0, \quad (x,y)\in(0,1)\times(0,1), \\ u(x,0) = \sin(2\pi x)\sin(2\pi y). \end{cases} \tag{4.1}$$

Table 1: Accurate test for the hybrid DG/WENO-FD method (Example 4.1).

N	$L_\infty(DG)$	$L_\infty(WENO)$	Order	$L_1(DG)$	$L_1(WENO)$	Order
1/20	6.33E-04	6.17E-04		1.13E-04	1.99E-04	
1/40	6.35E-05	4.08E-05	3.31	1.17E-05	9.16E-06	3.27
1/80	7.77E-06	5.07E-06	3.00	1.44E-06	7.24E-07	3.02
1/160	9.39E-07	7.51E-07	2.76	1.82E-07	7.41E-08	2.98

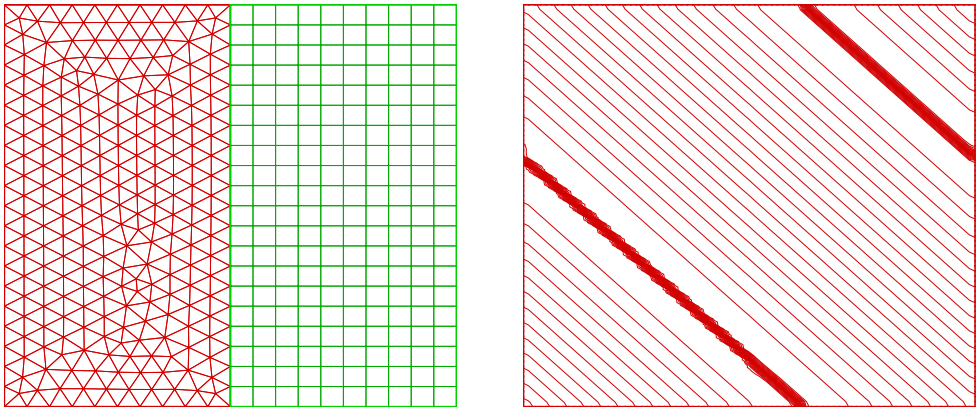

(a) Hybrid mesh ($h=1/20$) (b) Shock capture ($h=1/40$)

Figure 3: Sample hybrid mesh and shock capture for two dimensional burgers' equation.

Example 4.2. We further test the performance of the multi-domain hybrid DG/WENO-FD method for solving two dimensional inviscid burgers' equation with the following initial and periodic boundary conditions. The subdomain interface occurs at $x=0.0, -1.0<y<1.0$. The computing time is till $0.5/\pi$ and $1.5/\pi$. At $T=0.5/\pi$, the solution is still smooth. We display the L_∞ and L_1 errors of the DG and the WENO-FD subdomain, respectively. Numerical results show that accuracy is of third order accuracy as shown in Table 2. At $T=1.5/\pi$, the numerical results illustrate that shock waves can correctly pass through the coupling interface in Fig. 3(b).

$$\begin{cases} u_t+(\frac{u^2}{2})_x+(\frac{u^2}{2})_y=0, & (x,y)\in(-1,1)\times(-1,1), \\ u(x,0)=0.5\sin(\pi(x+y))+0.25. \end{cases} \tag{4.2}$$

Table 2: Accurate test for the hybrid DG/WENO-FD method (Example 4.2).

N	$L_\infty(DG)$	$L_\infty(WENO)$	Order	$L_1(DG)$	$L_1(WENO)$	Order
1/20	4.19E-03	6.09E-03		1.52E-04	1.01E-04	
1/40	8.11E-04	5.21E-05	2.37	1.42E-05	5.23E-05	3.42
1/80	6.09E-05	2.40E-06	3.73	1.67E-06	2.02E-06	3.08
1/160	4.97E-07	2.70E-07	3.15	2.16E-07	6.76E-08	2.95

4.2 Two dimensional Euler cases

We consider the two dimensional Euler equations:

$$U_t+F(U)_x+G(U)_y=0, \tag{4.3}$$

where $U=(\rho,\rho u,\rho v,E)^T$, $F(U)=(\rho u,\rho u^2+P,\rho uv,u(E+P))^T$, $G(U)=(\rho v,\rho uv,\rho v^2+P,u(E+P))^T$. The total energy E is expressed

$$E=\frac{P}{\gamma-1}+\frac{1}{2}\rho(u^2+v^2), \tag{4.4}$$

with $\gamma=1.4$ for ideal gas.

Example 4.3 (Double mach reflection)**.** This is a standard test case for high resolution schemes. The computational domain for this problem is chosen to be $[0,4]\times[0,1]$. Initially a right-moving Mach 10 shock is positioned at $x=1/6,y=0$ and makes a 60^o angle with the x-axis. The artificial interface is located at $y=0.2,0.0<x<4.0$ with the unstructured DG method computing 20% regions of total domain near the bottom. The numerical results are presented in Fig. 4 with a comparison among the traditional 3^{rd}-order RKDG method, the hybrid 3^{rd}-order DG/WENO-FD method using DG flux and the hybrid 3^{rd}-order DG/WENO-FD method using WENO-FD flux, respectively. A series of density contours are shown in Fig. 4. The hybrid solver using DG flux and using WENO-FD flux both get good resolution comparable with the 3^{rd}-order RKDG method, but we note that our hybrid method is more efficient than the traditional RKDG method which nearly 60% CPU time is saved in this test case. It should be noted that the DG flux with Lagrangian interpolation as proposed in our previous work did not work out for this case.

Example 4.4 (Interaction of isentropic vortex and weak shock wave)**.** This problem describes the interaction between a moving vortex and a stationary shock wave. The computational domain is taken to be $[0,2]\times[0,1]$. A stationary shock wave is located at $x=0.5$ with a shock Mach number 1.1. An isentropic vortex is superposed to flow left to the shock wave with the following conditions:

$$\delta u=\varepsilon\tau e^{\alpha(1-r^2)}\sin\theta, \tag{4.5a}$$

$$\delta v=-\varepsilon\tau e^{\alpha(1-r^2)}\cos\theta, \tag{4.5b}$$

$$\delta T=\frac{(\gamma-1)\varepsilon^2e^{2\alpha(1-r^2)}}{4\alpha\gamma}, \tag{4.5c}$$

$$\delta S=0, \tag{4.5d}$$

where $\tau=r/r_c$, $r=\sqrt{(x-x_c)^2+(y-y_c)^2}$, $(x_c,y_c)=(0.25,0.5)$. Here, ε describes the strength of the vortex, α is the decay rate of the vortex and r_c is the critical radius of maximum strength. For this test we choose $\varepsilon=0.3$, $\alpha=0.204$, $r_c=0.05$. We compare the performances among the traditional 3^{rd}-order RKDG method, the 3^{rd}-order hybrid DG/WENO-FD method using DG flux and 3^{rd}-order hybrid DG/WENO-FD method using WENO-FD flux, respectively. The coupling interface is located at $y=0.5,0.0<x<2.0$. Numerical results in Fig. 5 show that the resolution of hybrid DG/WENO-FD of both using DG flux and WENO flux is stable and comparable to the 3^{rd}-order RKDG method. However, in contrast to the 3^{rd}-order RKDG method, the 3^{rd}-order hybrid solver saves almost 45% CPU time with employing the hybrid strategy.

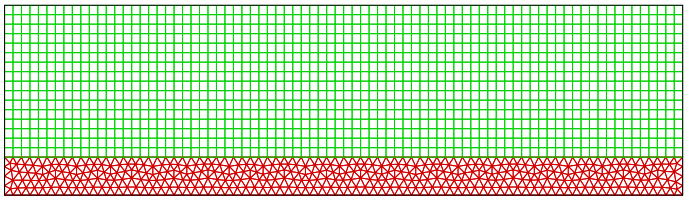

(a) Sample hybrid mesh, mesh size $h=1/20$.

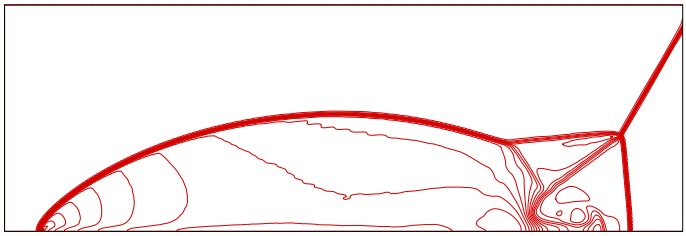

(b) 3^{rd}-RKDG method, density 30 contours from 1.731 to 20.92, mesh size h=1/120, t=0.2, CPU time: 92743.4s.

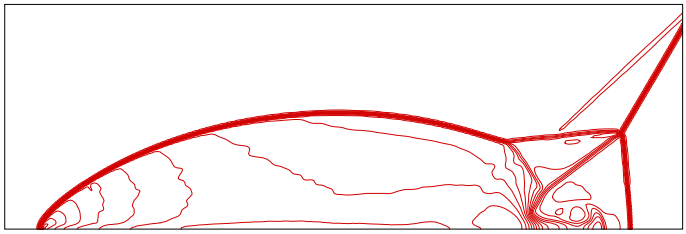

(c) 3^{rd}-hybrid DG/WENO-FD method (using DG flux), density 30 contours from 1.731 to 20.92, mesh size h=1/120, t=0.2, CPU time: 39757.3s.

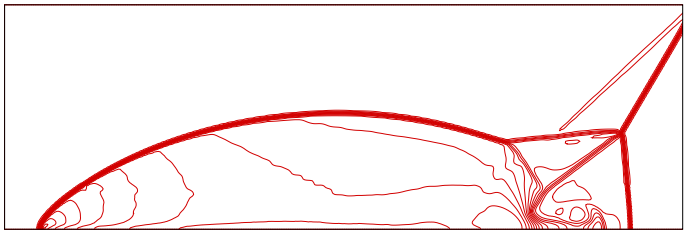

(d) 3^{rd}-hybrid DG/WENO-FD method (using WENO-FD flux), density 30 contours from 1.731 to 20.92, mesh size h=1/120, t=0.2, CPU time: 39894.4s.

Figure 4: Double mach reflection (Example 4.3).

Example 4.5 (Incident shock past a cylinder)**.** This example concerns the simulation of an incident shock wave interaction with a circular cylinder. The computational domain is a rectangle with length from $x=-1.5$ to $x=1.5$ and height for $y=-1.0$ to $y=1.0$ with a

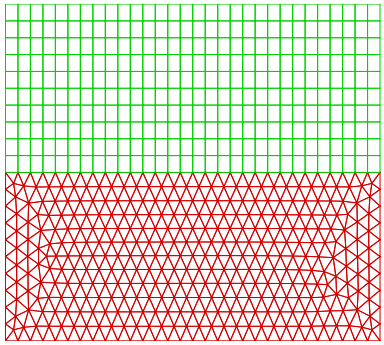

(a) Sample mesh, mesh size $h = 1/20$.

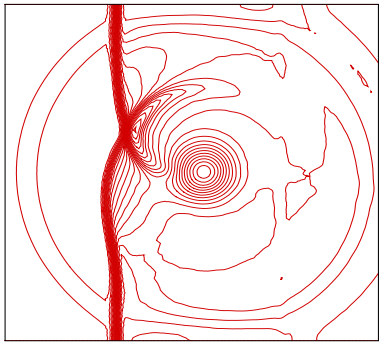

(b) 3^{rd}-RKDG method, density 30 contours from 1.0 to 1.24, mesh size h=1/100, t=0.4, CPU time: 4105.9s.

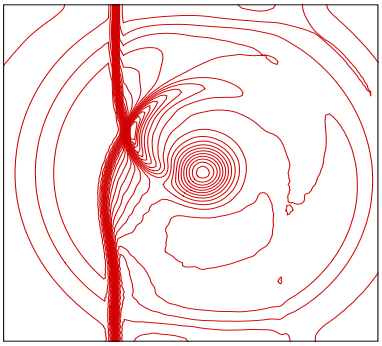

(c) 3^{rd}-hybrid DG/WENO-FD method (using DG flux), density 30 contours from 1.0 to 1.24, mesh size h=1/100, t=0.4, CPU time: 2073.6s.

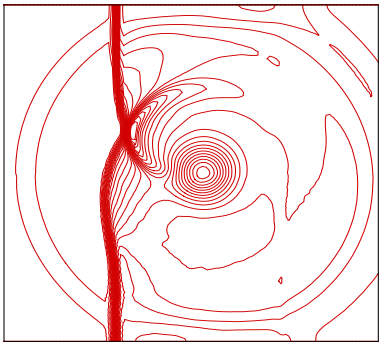

(d) 3^{rd}-hybrid DG/WENO-FD method (using WENO-FD flux), density 30 contours from 1.0 to 1.24, mesh size h=1/100, t=0.4, CPU time: 2148.7s.

Figure 5: Interaction of isentropic vortex and weak shock wave (Example 4.4).

cylinder at the center. The diameter of the cylinder is 0.25 and its center is located at $(0,0)$. The incident shock wave is of Mach number 2.81 and the initial discontinuity is placed at $x=-1.0$. We apply the unstructured DG method to handle curve boundaries in the sub-domain $[-0.5,0.5]\times[-0.5,0.5]$ with the structured WENO-FD scheme for other regions. The numerical results are presented in Fig. 6 with a comparison among the traditional 3^{rd}-order RKDG method, the hybrid 3^{rd}-order DG/WENO-FD method using DG flux and the hybrid 3^{rd}-order DG/WENO-FD method using WENO-FD flux, respectively. We can see both the hybrid solver with DG flux and the hybrid solver with WENO-FD flux show good performances in this case compared to the RKDG method, however, it should be noted that the CPU time of our hybrid method is only about $1/6$ of the traditional RKDG method.

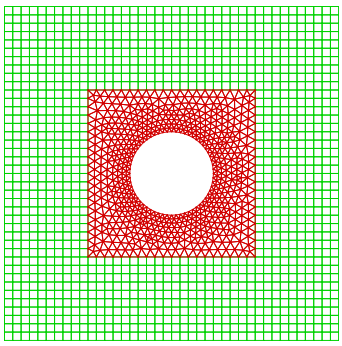

(a) Sample hybrid mesh, mesh size $h=1/20$.

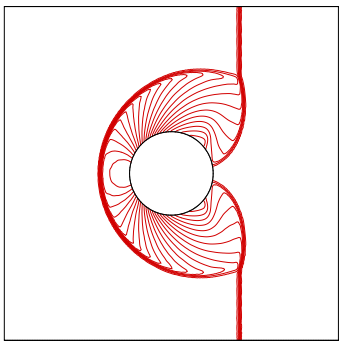

(b) 3^{rd}-RKDG method, pressure 25 contours from 1.0 to 20.0, mesh size h=1/100, t=0.5, CPU time: 41266.7s.

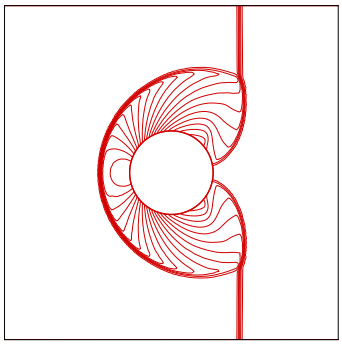

(c) 3^{rd}-hybrid DG/WENO-FD method (using DG flux), pressure 25 contours from 1.0 to 20.0, mesh size h=1/100, t=0.5, CPU time: 7219.6s.

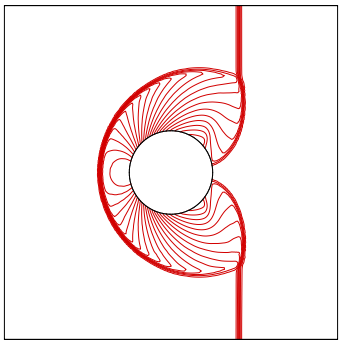

(d) 3^{rd}-hybrid DG/WENO-FD method (using WENO-FD flux), pressure 25 contours from 1.0 to 20.0, mesh size h=1/100, t=0.5, CPU time: 7100.6s.

Figure 6: Incident shock past a cylinder (Example 4.5).

Example 4.6 (Subsonic flow past a NACA0012 airfoil)**.** To demonstrate the flexibility in handling different geometries of the hybrid DG/WENO-FD method, we present a test case which a NACA0012 airfoil in the flow field with Mach number 0.4 and attack angle 5.0°. In this test case, unstructured meshes are applied in the domain $[-0.4,1.4]\times[-0.4,0.4]$ around the airfoil and structured meshes used other computational domains. Fig. 7(a) demonstrates a sample mesh of this test case with mesh size $h=1/10$. Fig. 7(b) and Fig. 7(c) show the pressure and density contours of the computational result of our hybrid solver with the entropy production on the airfoil surface shown in Fig. 7(d). Also, we present the Cp distribution and convergence history which are compared to the traditional third-order RKDG method in Fig. 7(e) and Fig. 7(f). The contour and Cp results by both methods has no much difference, however, a faster convergence was gained by the present hybrid method.

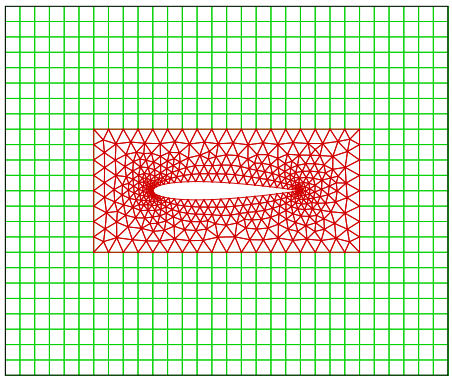

(a) Sample hybrid mesh, mesh size h=1/10.

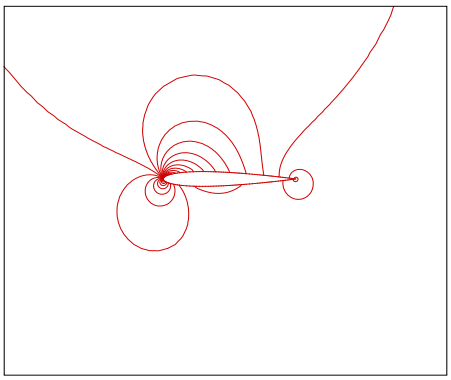

(b) 3^{rd}-hybrid DG/WENO-FD method, pressure 20 contours from 0.82 to 1.1, mesh size h=1/20.

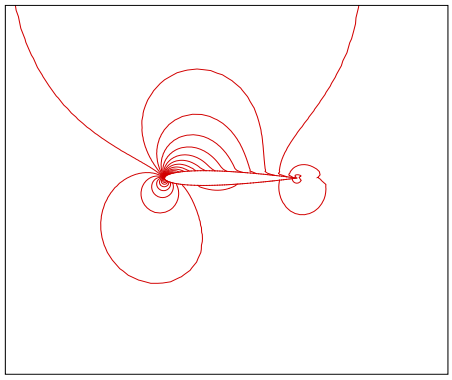

(c) 3^{rd}-hybrid DG/WENO-FD method, density 24 contours from 0.86 to 1.07, mesh size h=1/20.

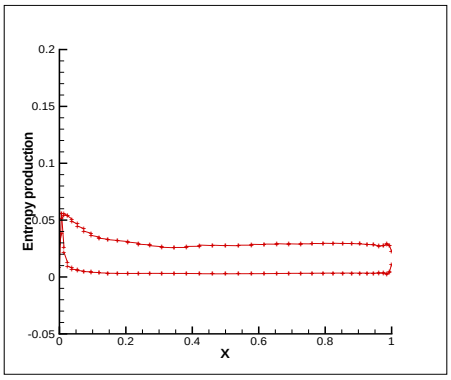

(d) Entropy production on the surface for the 3^{rd}-hybrid DG/WENO-FD method.

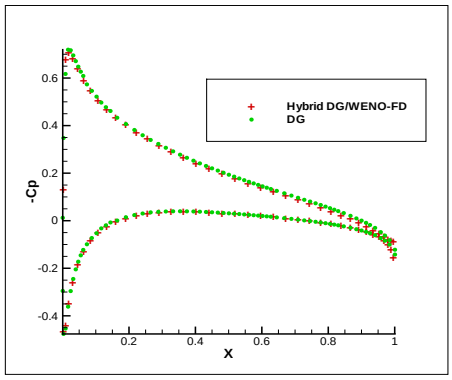

(e) Cp distribution comparison between the DG method and the hybrid DG/WENO-FD method.

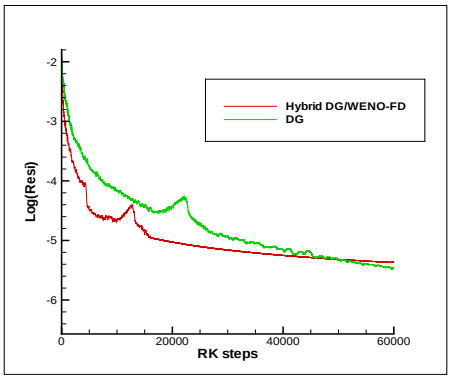

(f) Convergence history comparison between the DG method and the hybrid DG/WENO-FD method.

Figure 7: Subsonic flow past a NACA0012 airfoil (Example 4.6).

5 Concluding remarks

A robust approach of reconstructing DG flux based on WENO interpolation has been introduced. Numerical experiments show it is robust and stable when there is strong discontinuity passing through the coupling interface and can achieve good performance compared with the traditional RKDG methods. This provides us a flexible choice of selecting interface flux for the moment of conservative coupling. The resultant hybrid solver has demonstrated its flexibility in handling complex boundary geometries than a pure WENO-FD scheme and its capacity of saving computational cost compared with a traditional RKDG method. The stability analysis and the extension of the method to Navier-Stokes equations is undergoing.

Acknowledgments

This work is supported by the Innovation Foundation of BUAA for PhD Graduates, the National Natural Science Foundation of China (Nos. 91130019 and 10931004), the international cooperation project No. 2010DFR00700, the Fundamental Research of Civil Aircraft MJ-F-2012-04 and the National 973 project No. 2012CB720205.

References

[1] B. Cockburn, C.-W. Shu, TVB Runge-Kutta local projection discontinuous Galerkin finite element method for scalar conservation laws II: general framework, Math. Comp., 52 (1989), 411-435.
[2] B. Cockburn, C.-W. Shu, TVB Runge-Kutta local projection discontinuous Galerkin finite element method for scalar conservation laws III: one dimensional systems, J. Comput. Phys., 84 (1989), 90-113.
[3] B. Cockburn, C.-W. Shu, The Runge-Kutta local projection discontinuous Galerkin finite element method for scalar conservation laws V: multidimensional systems, J. Comput. Phys., 141 (1998), 199-224.
[4] J. Zhu, J. X. Qiu, C.-W. Shu, M. Dumbser, Runge-Kutta discontinuous Galerkin method using WENO limiters II: unstructured meshes, J. Comput. Phys., 227 (2008), 4330-4353.
[5] J. Zhu, J. X. Qiu, Hermite WENO schemes and their application as limiter for Runge-Kutta discontinuous Galerkin method III: unstructured meshes, J. Sci. Comput., 39 (2009), 293-321.
[6] H. Luo, J. D. Baum, R. Löhner, A Hermite WENO-based limiter for discontinuous Galerkin method on unstructed grids, J. Comput. Phys., 225 (2007), 686-713.
[7] G. S. Jiang, C.-W. Shu, Efficient implementation of weighted ENO schemes, J. Comput. Phys., 126 (1996), 202-228.
[8] C.-W. Shu, Essentially non-oscillatory and weighted essentially non-oscillatory schemes for hyperbolic conservation laws, NASA/CR-97-206253, ICASE Report No.97-65.
[9] O. Friedrich, Weighted essentially non-oscillatory schemes for the interpolation of mean values on unstructured grids, J. Comput. Phys., 144 (1998), 194-212.
[10] T. J. Barth, P. O. Frederickson, High-order solution of the Euler equations on unstructured grids using quadratic reconstruction, AIAA-1990-0013, 1990.

[11] D. S. Balsara, C. Altmann, C. D. Munz, M. Dumbser, A sub-cell based indicator for troubled zones in RKDG schemes and a novel class of hybrid RKDG+HWENO schemes, J. Comput. Phys., 226 (2007), 586-620.
[12] H. Luo, L. Q. Luo, R. Nourgaliev, A reconstructed discontinuous Galerkin method for the Euler equations on arbitrary grids., Commun. Comput. Phys., 12 (2012), 1495-1519.
[13] H. Luo, Y. D. Xia, R. Nourgaliev, C. P. Cai, A class of reconstructed discontinuous Galerkin methods for the compressible flows on arbitrary grids, AIAA-2011-0199, 2011.
[14] M. Dumbser, D. S. Balsara, E. F. Toro, A unified framework for the construction of one step finite volume and discontinuous Galerkin schemes on unstructed meshes, J. Comput. Phys., 227 (2008), 8209-8253.
[15] L. P. Zhang, W. Liu, L. X. He, X. G. Deng, H. X. Zhang, A new class of DG/FV hybrid methods for conservation laws I: basic formulation and one-dimensional systems, J. Comput. Phys., 231 (2012), 1081-1103.
[16] L. P. Zhang, W. Liu, L. X. He, X. G. Deng, H. X. Zhang, A class of hybrid DG/FV methods for conservation laws II: two dimensional cases, J. Comput. Phys., 231 (2012), 1104-1120.
[17] L. P. Zhang, W. Liu, L. X. He, X. G. Deng, A class of hybrid DG/FV methods for conservation laws III: two dimensional Euler Equations, Commun. Comput. Phys., 12 (2012), 284-314.
[18] L. P. Zhang, W. Liu, L. X. He, X. G. Deng, A new class of DG/FV hybrid schemes for one-dimensional conservation law, The 8th Asian Conference on Computational Fluid Dynamics, Hong Kong, 10-14 January, 2010.
[19] Z. J. Wang, Spectral (Finite) volume method for conservation laws on unstructured grids: basic formulation, J. Comput. Phys., 178 (2002), 210-251.
[20] Y. Liu, M. Vinokur, Z. J. Wang, Spectral difference method for unstructured grids I: basic formulation, J. Comput. Phys., 216 (2006), 780-801.
[21] Y. Sun, Z.J. Wang and Y. Liu, High-order multidomain spectral difference method for the Navier-Stokes equations on unstructured hexahedral grids, Commun. Comput. Phys., 2 (2007), 310-333.
[22] H. T. Huynh, A flux reconstruction approach to high-order schemes including discontinuous Galerkin methods, AIAA-2007-4079, 2007.
[23] B. Costa, W. S. Don, Multi-domain hybrid spectral-WENO methods for hyperbolic conservation laws, J. Comput. Phys., 224 (2007), 970-991.
[24] K. Shahbazi, N. Albin, O. P. Bruno, J. S. Hesthaven, Multi-domain Fourier-continuation/WENO hybrid solver for conservation laws, J. Comput. Phys., 230 (2011), 8779-8796.
[25] J. Cheng, Y. W. Lu, T. G. Liu, Multi-domain hybrid RKDG and WENO methods for hyperbolic conservation laws, SIAM J. Sci. Comput., 35(2) (2013), A1049-A1072.
[26] J. Utzmann, F. Lörcher, M. Dumbser, C.-D. Munz, Aeroacoustic simulations for complex geometries based on hybrid meshes, AIAA-2006-2418, 2006.
[27] J. Utzmann, T. Schwartzkopff, M. Dumbser, C.-D. Munz, Heterogeneous domain decomposition for computational aeroacoustics, AIAA jouirnal, 44(10) (2006), 2231-2250.
[28] R. Léger, C. Peyret, S. Piperno, Coupled discontinuous Galerkin/finite difference solver on hybrid meshes for computational aeroacoutics., AIAA journal, 50(2) (2012), 338-349.